Thermal-hydraulic assessment of the Steam Generator mock-up for the EU DEMO WCLL using CFD co-simulation

Fusion Engineering and Design 201 (2024) 114237

Contents lists available at ScienceDirect

Fusion Engineering and Design

journal homepage: www.elsevier.com/locate/fusengdes

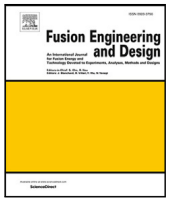

Thermal-hydraulic assessment of the Steam Generator mock-up for the EU DEMO WCLL using CFD co-simulation

D. Caterino [a], A. Del Nevo [b], M. Eboli [b], A. Froio [a,*], R. Marinari [b], A. Vannoni [c], A. Zappatore [a]

[a] NEMO group, Dipartimento Energia, Politecnico di Torino, Corso Duca degli Abruzzi 24, 10129, Torino (TO), Italy
[b] ENEA CR Brasimone, Fusion and Technology for Nuclear Safety and Security Department, 40032, Comugnano (BO), Italy
[c] Department of Astronautical, Electrical and Energy Engineering, Sapienza University of Rome, Corso Vittorio Emanuele II 244, 00186, Roma (RM), Italy

ARTICLE INFO

Keywords:
EU DEMO
WCLL
CFD
Steam generator
Thermal-hydraulics
Co-simulation

ABSTRACT

The Primary Heat Transfer System (PHTS) of the EU DEMO Water-Cooled Lithium-Lead (WCLL) Breeding Blanket might rely on Once-Through Steam Generators (OTSGs) technology, widely used in fission industry.

ENEA is currently developing the STEAM facility, in order to characterize the behaviour of the EU DEMO OTSG. To this aim, a dedicated OTSG mock-up is being designed.

The present work describes the Computational Fluid Dynamics (CFD) approach used to investigate the flow field within the inlet and outlet regions of the OTSG mock-up in steady-state conditions.

One of the key objectives of the analysis is to assess the mass flow distribution within the OTSG primary bundle, as uniform distribution is crucial for achieving the desired performance.

To this aim, the computational approach employs reliable models such as RANS $k-\epsilon$ as well as a fluid–fluid co-simulation routine. The aim is to reach a satisfactory self-consistency of the flow distribution within the OTSG primary bundle without the discretization of the full geometry.

The CFD analysis predicts a maximum absolute deviation from the average mass flow rate value lower than 2%. This predicted behaviour is compared against a benchmark simulation that discretizes the whole primary bundle. The comparison displays an acceptable compatibility and a significant reduction in the required computational resources thanks to the implementation of a co-simulation routine.

1. Introduction

The EU DEMO is planned to be a tokamak fusion reactor to deliver electricity in the EU [1]. It will feature a balance-of-plant (BoP) [2] to convert the power generated by the fusion reactions into electricity. The design of the Primary Heat Transfer System (PHTS) for the EU DEMO Water-Cooled Lithium-Lead (WCLL) Breeding Blanket [3] can take advantage of the large experience from light water fission reactors, but new challenges arise due to the intermittent operation (pulse-dwell-pulse regime) of the EU DEMO.

STEAM will be a novel experimental infrastructure operated by ENEA in order to validate the design of the BoP of the WCLL Breeding Blanket of the EU DEMO. As a part of the STEAM infrastructure tests, a Once-Through Steam Generator (OTSG) mock-up is currently being designed [4].

The purpose of the present work is to analyse the flow distribution within the OTSG mock-up to support its design process using state-of-the art computational models. The next section briefly describes the most significant design features in order to understand the computational approach and the co-simulation routine at the core of the study. Finally, the main results are discussed and then compared against a benchmark simulation. Additionally, the computational performances are evaluated in order to highlight the benefits of the implementation of the co-simulation routine.

2. OTSG mock-up design features

This section summarizes the most significant design characteristics of the OTSG. All mentioned values (e.g. mass flow rates, pressures and temperatures) are taken from the RELAP5/Mod3.3 OTSG model described in detail in [5,6].

The OTSG mock-up, presented in Fig. 1, consists of a 13.50 m long tube with a maximum outer diameter of 219 mm.

A magnetic drive centrifugal pump generates a maximum mass flow rate of 20 kg/s while an electrical heater heats the primary fluid up to 328 °C; a pressurizer sets the pressure of the circuit to 15.50 MPa. As a result, pressurized water flows downward entering from the inlet nozzle at a temperature of 328 °C. The primary bundle consists of 37

* Corresponding author.
E-mail addresses: danilo.caterino@polito.it (D. Caterino), antonio.froio@polito.it (A. Froio).

https://doi.org/10.1016/j.fusengdes.2024.114237
Received 13 October 2023; Received in revised form 25 January 2024; Accepted 8 February 2024
Available online 13 February 2024

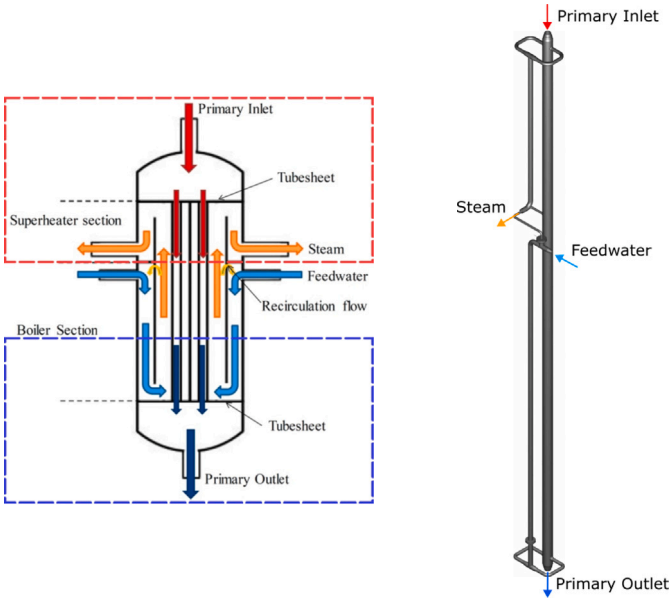

(a) OTSG conceptual scheme, highlighting the *TOP* and *BOTTOM* regions modelled in this work (red and blue boxes, respectively) [2].

(b) OTSG mock-up layout.

Fig. 1. OTSG conceptual scheme (Fig. 1(a)) and the OTSG mock-up layout (Fig. 1(b)).

Table 1
Operating conditions for each OTSG region.

Region	Fluid	P [MPa]	T [°C]	$\dot{m}$ [kg/s]
OTSG TOP Primary	Liquid water	15.50	328	15.0
OTSG BOTTOM Primary	Liquid water	15.42[a]	295	15.0
OTSG TOP Secondary	Superheated steam	6.36[b]	300	1.64
OTSG BOTTOM Secondary	Liquid water	6.40	238	1.86

[a] Value calculated from CFD model.
[b] Value calculated from RELAP5/Mod3.3 model.

Table 2
Prism layer mesher settings.

	Number of layers	Near wall layer thickness [mm]	Total thickness [mm]
Primary pipes - inner	10	0.075	3.0
Primary pipes - outer	8	0.12	1.5
Riser	8	0.12	1.5
Everywhere else	10	0.075	3.0

smaller pipes to maximize the efficiency of the heat exchange with the secondary fluid. Each primary pipe has an outer diameter of 15.88 mm. The design temperature at the primary outlet is 295 °C.

Four magnetic drive centrifugal pumps create a mass flow rate of approximately 1.64 kg/s within the secondary side. As a result, subcooled water enters the feedwater downcomer at a temperature of 238 °C and a pressure of 6.40 MPa and flows downwards. After reaching the riser, the secondary fluid starts to flow upwards while approaching saturated conditions. Phase change from liquid to vapour occurs along the riser and, as a result, superheated steam exits through the secondary outlet at an estimated temperature of 300 °C.

3. Model

The goal of the CFD analysis is to assess the flow behaviour near the primary and secondary inlets and outlets under steady-state conditions, while saving as much computational resources as possible. Therefore, the implemented simulation strategy aims at simplifying the geometry whilst capturing the most relevant physical phenomena with acceptable reliability.

The model was developed with the Simcenter STAR-CCM+ v2021.2.1-R8 commercial CFD software [7].

3.1. Geometry

The simulated OTSG mock-up geometry incorporates those areas of the secondary riser in which only one phase is present (e.g. superheated steam, and liquid water). Namely, the two areas of the secondary side are: the *OTSG TOP secondary* in which 100% superheated steam flows (red box in Fig. 1(a)), and the *OTSG BOTTOM secondary* in which 100% sub-cooled liquid water flows (blue box in Fig. 1(a)).

Consequently, the primary bundle was also split into two parts adjacent to the respective secondary parts: the *OTSG TOP primary* and the *OTSG BOTTOM primary*. In this way, the two OTSG secondary parts can be solved without the implementation of a phase-change model.

Table 1 summarizes the operating conditions within all the resulting four regions of the OTSG mock-up.

3.2. Meshing approach

The computational model takes advantage of the symmetric flow distribution at the primary and secondary inlets and of the whole secondary riser geometry. Therefore, a symmetric condition along the $x = 0$ plane (with reference to the coordinate system displayed in Fig. 2(a)) was deemed feasible, according to the expected results, and enforced within the physical domain to guarantee a significant reduction in the overall cell count. As a result, only half of each domain was simulated and the correspondent total mass flow rates (in Table 1) were halved accordingly.

The simulated OTSG geometry employs approximately 43 million hexahedral cells, including prismatic cells used to resolve the boundary layer. The main settings used for the prism layer mesher are listed in Table 2. Mesh quality was evaluated taking into account the *face validity*, the *volume change* and the *skewness angle*. The methodology and the following threshold values were chosen according to the STAR-CCM+ User Guide [7]. The evaluation reports that: 99.99% of the

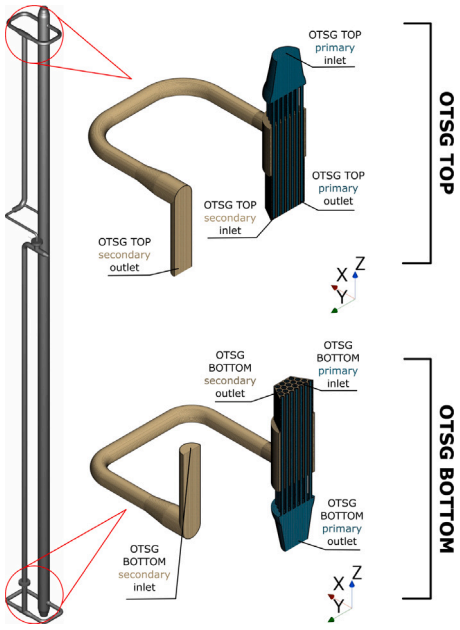

(a) OTSG mock-up (left) and simulated geometry (right).

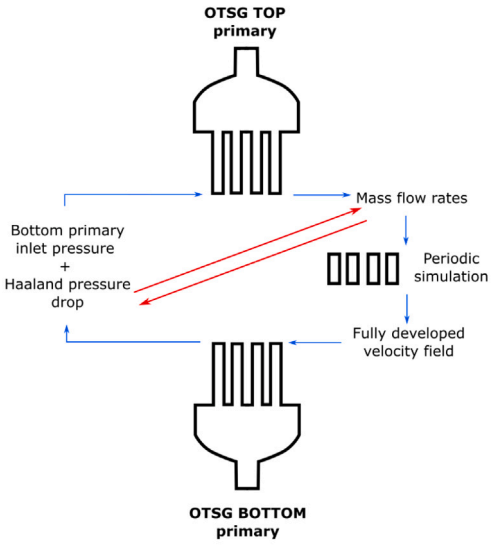

(b) Co-simulation routine.

Fig. 2. OTSG geometry (Fig. 2(a)) and co-simulation routine diagram (Fig. 2(b)).

generated cells have a face validity equal to 1.0, 100% a volume change higher than 0.01, and 99.91% a skewness angle lower than 85°.

Fig. 2(a) shows the discretized regions and highlights the inlets and outlets of each computational domain.

3.3. Co-simulation routine

Early analyses demonstrated that different pressure is exerted at the outlet boundary of each top primary pipe. Moreover, non-uniform velocity distribution at the *OTSG TOP primary* inlet induces different mass flow rates within each pipe. Hence, pressure drop along each pipe is different and it affects flow distribution within the *OTSG BOTTOM primary*. Therefore, it was necessary to employ a co-simulation routine able to reach a satisfactory phenomenon representation by coupling each primary top pipe with its bottom counterpart. This would also avoid meshing and computing the solution in the entire length of straight pipes of the primary. The overall length of the simulated domain is, in fact, around 1.29 m, less than one tenth of the whole mock-up extension (see Section 2).

The chosen co-simulation routine, sketched in Fig. 2(b), consists of two parallel subroutines: an outer routine (red loop) and an inner routine (blue loop).

3.3.1. Outer routine

The outer routine exchanges velocity field information from top to bottom and pressure field information from bottom to top in order to achieve a satisfactory consistency of the flow distribution within the primary.

This routine exploits the mass flow rate within each top primary pipe to derive a fully developed velocity field at the working conditions of the OTSG bottom primary.

The resulting velocity field is assigned to the inlet boundary of the correspondent bottom primary pipe.

Pressure exerted at the inlet boundary of each bottom primary pipe $p_{in_i}^{bot}$ is added to the pressure drop contribution Δp_{DW_i} estimated by the inner routine.

The resulting pressure $p_{out_i}^{top}$ is assigned to the outlet boundary of the correspondent top primary pipe following Eq. (1):

$$p_{out_i}^{top} = p_{in_i}^{bot} + \Delta p_{DW_i}, \tag{1}$$

where $p_{in_i}^{bot}$ is the pressure of the correspondent bottom primary pipe and Δp_{DW_i} is the estimated pressure drop.

Physics of all OTSG parts is then solved under these new boundary conditions and, as a result, a new mass flow rate distribution is calculated.

The outer routine is outlined in Fig. 2(b) by the blue loop and enacted every 1200 iterations; no significant impact on convergence was observed in the range 800–1200 iterations.

3.3.2. Inner routine

The inner routine estimates pressure drop along each pipe Δp_{DW_i} using the Darcy–Weisbach equation (2), namely:

$$\Delta p_{DW_i} = f_{D_i} \frac{\overline{\rho}}{2} \frac{\overline{v}_i^2}{D_H}. \tag{2}$$

The hydraulic diameter D_H is known from the OTSG mock-up geometry features (see Section 2) and average density $\overline{\rho}$ can be estimated from conditions in Table 1. Whereas, the average velocity within each pipe $\overline{v}_i$ is derived from mass flow rate distribution. The Darcy friction factor f_{D_i} is estimated thanks to the implementation of the explicit Haaland formula [8], specifically:

$$\frac{1}{\sqrt{f_{D_i}}} = -1.8 \log \left[\left(\frac{\varepsilon / D_H}{3.7} \right)^{1.11} + \frac{3.9}{Re_i} \right], \tag{3}$$

where ε is the pipe absolute roughness determined by the material and cross-section shape (e.g. stainless steel, circular pipe): $\varepsilon = 0.02$ mm; Re_i is the Reynolds number calculated using the averaged fluid properties (e.g. $\overline{\rho}$, $\overline{\mu}$), the hydraulic diameter D_H, and the average velocity within each pipe $\overline{v}_i$ (derived from the mass flow rate within the same pipe).

The inner routine is outlined in Fig. 2(b) by the red loop and enacted every 50 iterations, which represents the minimum threshold. Below this limit, the simulation starts to experience numerical instability.

3.4. Boundary conditions, initial conditions and turbulence model

Fully-developed pipe flow conditions are applied to both secondary inlets. The top primary inlet is not fully-developed (due to the upstream presence of a u-bent pipe which is not included in the current OTSG

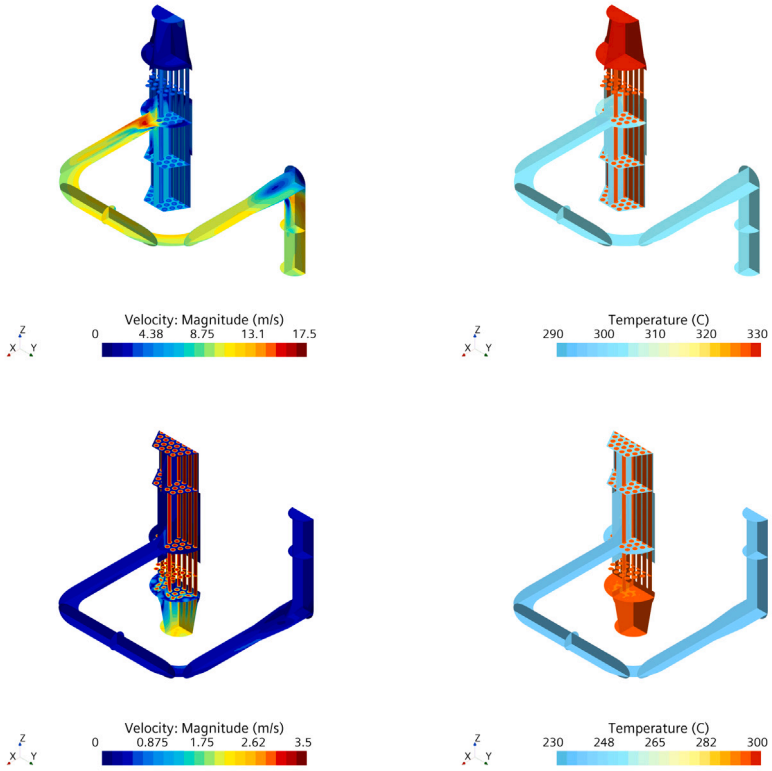

(a) Scalar field of the velocity magnitude at different section planes.

(b) Scalar field of the temperature at different section planes.

Fig. 3. Main field distributions, namely velocity (Fig. 3(a)) temperature (Fig. 3(b)), represented using multiple section planes.

geometry), therefore its boundary conditions were computed with a dedicated simulation. Bottom primary inlet conditions are managed by the co-simulation routine since they are strongly influenced by the flow distribution within the top primary region.

Relative pressure for both secondary outlets and for the bottom primary outlet is set to 0 Pa. Pressure distribution at the top primary outlet is calculated by the co-simulation routine as described in Section 3.3.

Initial pressure at the top primary outlet is set to a uniform distribution calculated using Eqs. (1)–(3) with $p_{in_i}^{bot} = 0$ Pa, and an initial velocity calculated as:

$$\overline{v}_i^{initial} = \frac{4\dot{m}_{tot}}{37\pi\overline{\rho}D_H^2}. \tag{4}$$

Fluid properties depend on temperature through IAPWS-IF97 [9] standard. Heat transfer is, in fact, allowed between the primary and the secondary thanks to an interface that models the stainless steel thermal resistance.

Reynolds-averaged Navier–Stokes equations (RANS) coupled with $\kappa - \epsilon$ [10] turbulence model and all-y^+ wall treatment are solved in order to assess the mean flow field.

4. Main results

Once mass flow rate within each primary pipe had reached a satisfactory convergence, the results regarding the distribution of the main fields were analysed.

4.1. Velocity and temperature distribution results

Fig. 3(a) shows that high velocity gradients are located within the OTSG top secondary, where the magnitude of the velocity of the superheated steam reaches its maximum value of approximately 17.5 m/s.

Whereas, Fig. 3(b) indicates that temperature field is approximately uniform in each OTSG region, as a result of the assumptions described in Section 3.1.

4.2. Mass flow rate distribution results

The co-simulation predicts a slightly non-uniform mass flow distribution within the 37 primary pipes, as reported in Fig. 4(a). This non-homogeneity was evaluated through the representation of the deviation percentage from the average mass flow rate ϵ_i for each pipe and shown in Fig. 4(b). The definition of ϵ_i states as follows (Eq. (5)):

$$\epsilon_i = \frac{\dot{m}_i - \overline{\dot{m}}}{\overline{\dot{m}}} \cdot 100, \tag{5}$$

where $\dot{m}_i$ is the mass flow rate calculated within a single pipe and $\overline{\dot{m}}$ is the average mass flow rate. Fig. 4(b) shows that:

- Pipes 5, 13, 14, 15, 16, 17 experience a mass flow rate higher than the average value, with a deviation approximately equal to or higher than +0.5%,
- Pipes 9, 21, 22, 23 experience a mass flow rate lower than the average value, with a deviation approximately equal to or lower than −0.5%,
- All the other pipes experience a mass flow rate within ±0.5% of the average value,
- Overall, all deviation values lie between ±2%.

Mass flow rate distribution is strongly influenced by non fully-developed conditions at the top primary inlet mentioned in Section 3.4.

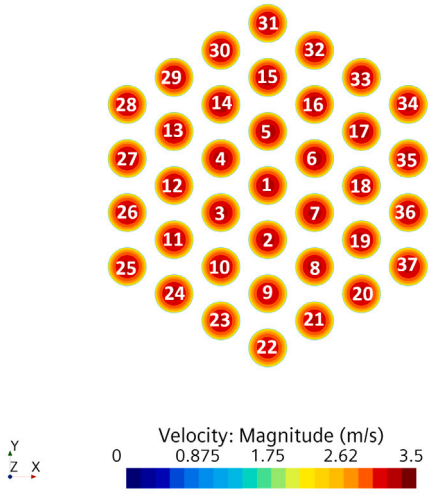

(a) Scalar field of the velocity magnitude within primary pipes (mirrored).

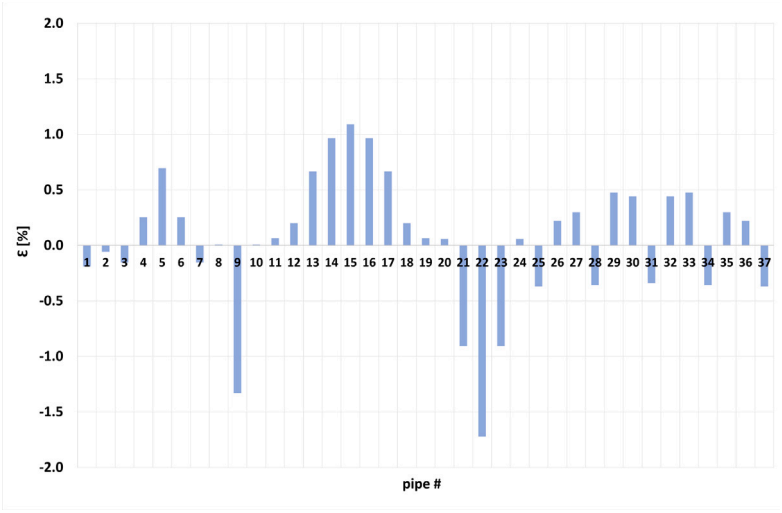

(b) Single pipe mass flow rate deviation from average value.

Fig. 4. Velocity magnitude representation within each numbered pipe (Fig. 4(a)), and mass flow distribution (Fig. 4(b)).

4.3. Results and performance benchmark

The mass flow rate behaviour was compared against the results yielded by a benchmark simulation that discretizes the whole primary bundle using the same meshing approach employed in the co-simulation (without, however, enforcing a symmetric solution). Prism layer mesher settings used in the benchmark simulation are the same as the ones reported in Table 2 for the co-simulation.

As a result, the simulation of the complete primary uses approximately 130 million hexahedral cells to represent the physical domain. Mesh quality of the benchmark simulation was evaluated employing the same methodology mentioned in Section 3.2. The evaluation reports that: 99.99% of the generated cells have a face validity equal to 1.0, 100% a volume change higher than 0.01, and 99.99% a skewness angle lower than 85°. These results display a satisfactory consistency with the mesh quality of the co-simulation (described in Section 3.2).

Table 3 shows that 78% compatibility is achieved in the comparison of the qualitative mass flow rate behaviour. Overall, Table 3 highlights an under-prediction of the deviation modulus calculated using the co-simulation mass flow rate distribution. Specifically, the co-simulation under-prediction involves the outermost pipes of the primary bundle (pipe 25 and pipes from 28 to 37, see Fig. 4(a)). Finally, the complete primary simulation yielded absolute deviation values lower than 2% for all pipes with the exception of pipe 22, whose value is approximately 2.4%.

Performance analyses were performed using 4xIntel® Xeon® 8160 (SkyLake) at 2.10 GHz (192 cores in total) in order to assess the computational cost for both simulations. Fig. 5(a) shows the rate of change of the mass flow rate as a function of the number of iterations. For the sake of clarity, the chart only shows the rate of change of mass flow rate values whose convergence occurred last: specifically, mass flow rate within pipe 32 (and 30 due to symmetry) for the co-simulation, and mass flow rate within pipe 18 for the complete primary simulation. Fig. 5(a) indicates that an acceptable rate of change per iteration is achieved in approximately 10000 iterations. Namely, the complete primary simulation reaches a rate of change of 2% at approximately 5700 iterations, whereas the co-simulation reaches the same rate at approximately 8000 iterations. Curve slope suggests, in fact, that convergence speed of the complete primary simulation, in terms of required number of iterations, is higher. However, Fig. 5(b)

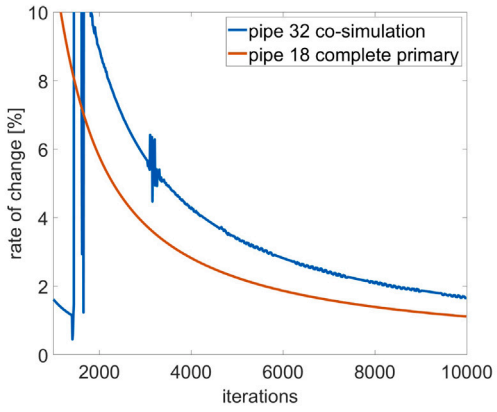

(a) Worst-case convergence of the mass flow rate.

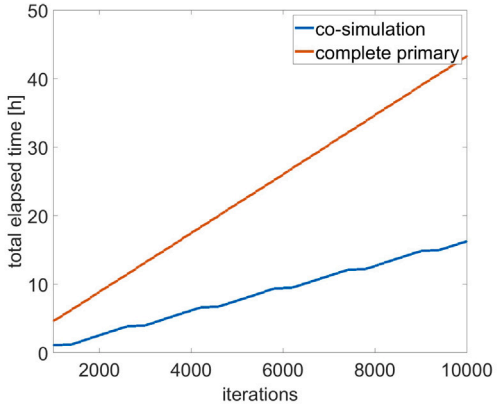

(b) Total elapsed time as a function of the number of iterations.

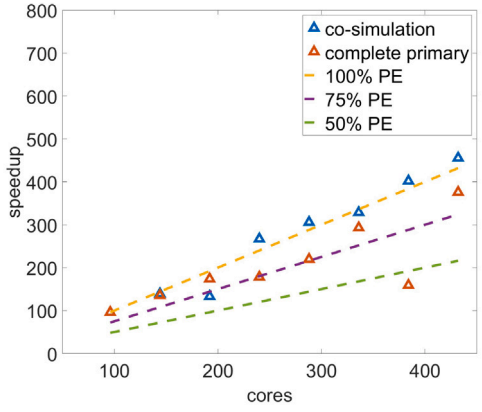

(c) Scalability tests and parallel efficiency.

Fig. 5. Benchmark of the co-simulation performances.

highlights that the total elapsed time required by the co-simulation to reach a 2% rate of change is half of the time required by the complete primary simulation to achieve the same rate. Namely, the complete primary simulation yielded stable results in 25 hours against the 13 hours needed by the co-simulation. Moreover, the maximum memory demanded during the computation for the co-simulation and the complete primary simulation is 139 GB and 234 GB, respectively.

Table 3
Mass flow rate distribution benchmark.

Pipe #	$\epsilon_i \geq \lvert 0.5 \rvert$ %	
	Co-simulation	Complete
1	x	x
2	x	x
3	x	x
4	x	x
5	✓	✓
6	x	x
7	x	x
8	x	x
9	✓	✓
10	x	x
11	x	x
12	x	x
13	✓	✓
14	✓	✓
15	✓	✓
16	✓	✓
17	✓	✓
18	x	x
19	x	x
20	x	x
21	✓	✓
22	✓	✓
23	✓	✓
24	x	x
25	x	✓
26	x	x
27	x	x
28	x	✓
29	x	✓
30	x	✓
31	x	x
32	x	✓
33	x	✓
34	x	✓
35	x	x
36	x	x
37	x	✓

Scalability of both simulations was tested and compared using 2xIntel® Xeon® 8160 (SkyLake) at 2.10 GHz (96 cores in total) as timing reference. The results are presented in Fig. 5(c). The co-simulation displays a parallel efficiency of around 100% against the 75% of the complete primary simulation.

5. Conclusions and future perspective

The CFD analysis of the OTSG mock-up for the STEAM facility was performed employing a co-simulation between the two furthermost parts of the heat exchanger. The central part was replaced by a pressure drop computed using well-documented formulae. The co-simulation highlighted a slight non-uniformity in the mass flow rate distribution within the 37 pipes of the OTSG primary side. Overall, mass flow rate values do not exceed the range between ± 2% of the average value.

Results and performance were compared against a similar CFD analysis which, however, discretizes the full primary bundle geometry. The co-simulation showed an acceptable accuracy in the prediction of the mass flow rate distribution within the 37 pipes. The main advantage in the implementation of the co-simulation routine lies in the significant reduction of the overall computational cost. Moreover, a good scalability on CPU nodes is achieved by the co-simulation.

Future analyses will be focused on multiple sensitivity tests encompassing different physics models and meshing strategies. Furthermore, upcoming studies will evaluate the potential impact of the predicted non-uniformity of the mass flow distribution on the OTSG performance.

CRediT authorship contribution statement

D. Caterino: Data curation, Formal analysis, Methodology, Software, Validation, Visualization, Writing – original draft. **A. Del Nevo:** Funding acquisition, Project administration. **M. Eboli:** Conceptualization, Funding acquisition, Project administration. **A. Froio:** Conceptualization, Methodology, Resources, Supervision, Writing – review & editing. **R. Marinari:** Project administration. **A. Vannoni:** Project administration. **A. Zappatore:** Conceptualization, Methodology, Resources, Supervision, Writing – review & editing.

Declaration of competing interest

The authors declare that they have no known competing financial interests or personal relationships that could have appeared to influence the work reported in this paper.

Data availability

Data will be made available on request.

Acknowledgements

This work has been carried out within the framework of the EUROfusion Consortium, funded by the European Union via the Euratom Research and Training Programme (Grant Agreement No. 101052200 – EUROfusion). Views and opinions expressed are however those of the author(s) only and do not necessarily reflect those of the European Union or the European Commission. Neither the European Union nor the European Commission can be held responsible for them. The work of AZ is financially supported by a EUROfusion Researcher Grant.

Computational resources were provided by HPC@POLITO, a project of Academic Computing within the Department of Control and Computer Engineering at the Politecnico di Torino (http://www.hpc.polito.it).

References

[1] A.J.H. Donné, W. Morris, X. Litaudon, C. Hidalgo, D. McDonald, H. Zohm, E. Diegele, A. Möslang, K. Nordlund, G. Federici, P. Sonato, C. Waldon, D. Borba, P. Helander, European Reasearch Roadmap to the Realisation of Fusion Energy, Tech. Rep., EUROfusion Consortium, ISBN: 978-3-00-061152-0, 2018.

[2] L. Barucca, W. Hering, S. Perez Martin, E. Bubelis, A. Del Nevo, M. Di Prinzio, M. Caramello, A. D'Alessandro, A. Tarallo, E. Vallone, I. Moscato, A. Quartararo, S. D'amico, F. Giannetti, P. Lorusso, V. Narcisi, C. Ciurluini, M.J. Montes Pita, C. Sánchez, A. Rovira, D. Santana, P. Gonzales, R. Barbero, M. Zaupa, M. Szogradi, S. Normann, M. Vaananen, J. Ylatalo, M. Lewandowska, L. Malinowski, E. Martelli, A. Froio, P. Arena, A. Tincani, Maturation of critical technologies for the DEMO balance of plant systems, Fusion Eng. Des. 179 (2022) 113096, http://dx.doi.org/10.1016/j.fusengdes.2022.113096, URL https://www.sciencedirect.com/science/article/pii/S0920379622000965.

[3] A. Del Nevo, P. Arena, G. Caruso, P. Chiovaro, P.A. Di Maio, M. Eboli, F. Edemetti, N. Forgione, R. Forte, A. Froio, F. Giannetti, G. Di Gironimo, K. Jiang, S. Liu, F. Moro, R. Mozzillo, L. Savoldi, A. Tarallo, M. Tarantino, A. Tassone, M. Utili, R. Villari, R. Zanino, E. Martelli, Recent progress in developing a feasible and integrated conceptual design of the WCLL BB in EUROfusion project, Fusion Eng. Des. 146 (2019) 1805–1809, http://dx.doi.org/10.1016/j.fusengdes.2019.03.040, SI:SOFT-30. URL https://www.sciencedirect.com/science/article/pii/S0920379619303503.

[4] A. Tincani, C. Ciurluini, A. Del Nevo, F. Giannetti, A. Tarallo, C. Tripodo, A. Cammi, A. Vannoni, M. Eboli, T. Del Moro, P. Lorusso, L. Barucca, Conceptual design of the steam generators for the EU DEMO WCLL reactor, Energies 16 (6) (2023) http://dx.doi.org/10.3390/en16062601, URL https://www.mdpi.com/1996-1073/16/6/2601.

[5] C. Ciurluini, A. Vannoni, T. Del Moro, P. Lorusso, A. Tincani, A. Del Nevo, L. Barucca, F. Giannetti, Thermal-hydraulic assessment of once-through steam generators for EU-DEMO WCLL breeding blanket primary cooling system application, Fusion Eng. Des. 193 (2023) 113688, http://dx.doi.org/10.1016/j.fusengdes.2023.113688, URL https://www.sciencedirect.com/science/article/pii/S0920379623002715.

[6] A. Vannoni, P. Lorusso, M. Eboli, F. Giannetti, C. Ciurluini, A. Tincani, R. Marinari, A. Tarallo, A. Del Nevo, Development of a steam generator mock-up for EU DEMO fusion reactor: Conceptual design and code assessment, Energies 16 (9) (2023) http://dx.doi.org/10.3390/en16093729, URL https://www.mdpi.com/1996-1073/16/9/3729.

[7] Siemens, Star-CCM+ v2021.2.1 user's manual, 2021, URL https://plm.sw.siemens.com/en-US/simcenter/fluids-thermal-simulation/star-ccm/.

[8] S.E. Haaland, Simple and explicit formulas for the friction factor in turbulent pipe flow, J. Fluids Eng. 105 (1) (1983) 89–90, http://dx.doi.org/10.1115/1.3240948, URL http://dx.doi.org/10.1115/1.3240948.

[9] W. Wagner, J.R. Cooper, A. Dittmann, J. Kijima, H.J. Kretzschmar, A. Kruse, R. Mares, K. Oguchi, H. Sato, I. Stocker, O. Sifner, Y. Takaishi, I. Tanishita, J. Trubenbach, T. Willkommen, The IAPWS industrial formulation 1997 for the thermodynamic properties of water and steam, J. Eng. Gas Turbines Power 122 (1) (2000) 150–184, http://dx.doi.org/10.1115/1.483186.

[10] T.-H. Shih, W.W. Liou, A. Shabbir, Z. Yang, J. Zhu, A new $\kappa-\epsilon$ eddy viscosity model for high Reynolds number turbulent flows, Comput. & Fluids 24 (3) (1995) 227–238, http://dx.doi.org/10.1016/0045-7930(94)00032-T, URL https://www.sciencedirect.com/science/article/pii/004579309400032T.